*J. Phys. Chem. A* **2001,** *105,* 11144−11155

# Hydrogen Atom Adducts to the Amide Bond. Generation and Energetics of the Amino(hydroxy)methyl Radical in the Gas Phase

**Erik A. Syrstad and František Tureček***

*Department of Chemistry, Bagley Hall, Box 351700, University of Washington, Seattle, Washington 98195-1700*

*Received: July 31, 2001; In Final Form: October 5, 2001*

The amino(hydroxy)methyl radical (**1**) represents the simplest model for hydrogen atom adducts to the amide bond. Radical **1** was generated in the gas phase by femtosecond electron transfer to protonated formamide and found to be stable on the microsecond time scale. The major unimolecular dissociation of **1** was loss of the hydrogen atom from the hydroxyl group. Losses of hydrogen atoms from the CH and $NH_2$ groups in **1** were less abundant. RRKM calculations on the G2(MP2), G2, and CCSD(T)/aug-cc-pVTZ potential energy surfaces predicted preferential loss of the hydroxyl hydrogen atom, in qualitative agreement with experiment. Bimolecular reactions of hydrogen atoms with formamide were predicted by calculations to prefer H atom abstraction from the H−C bond forming $H_2$ and $NH_2C{=}O^{\bullet}$. This reaction was calculated to be 43 kJ/mol exothermic and had to overcome an activation energy barrier of 28.5 kJ/mol. Hydrogen atom additions to the carbon and oxygen termini of the carbonyl group in formamide had similar activation energies, 51 and 49 kJ/mol, respectively. H atom addition to the C-terminus producing the aminomethyloxy radical (**6**) was calculated to be 2 kJ/mol endothermic.

## Introduction

Reactions of free radicals with biomolecules (nucleobases,[1] carbohydrates,[2] proteins,[3] lipids,[4] etc.) usually comprise additions to unsaturated bonds or hydrogen atom abstractions. Proteins, in particular, react by hydrogen atom abstraction from the backbone,[5] or reactive side chain groups such as the cysteine thiol group and the tyrosine hydroxyl group.[6] Intermediates of protein radical reactions have been investigated in the condensed phase,[3] and amino acid radicals have also been generated and investigated by mass spectrometry in the gas phase.[7] A notable exception to the usual protein radical reactivity, which was observed for gas phase ions trapped in an ion-cyclotron resonance mass spectrometer, is the backbone cleavage that occurs upon electron capture in multiply charged peptide and protein cations, termed electron capture dissociation (ECD).[8] The processes thought to operate in ECD are triggered by capture of a thermal electron by the multiply protonated peptide or protein in the rarefied gas phase. Since protonation in multiply charged gaseous protein ions is thought to occur predominantly at the highly basic amine and guanidine groups,[8] reduction by electron attachment of the primary ammonium group of a protonated lysine residue produces initially a transient hypervalent ammonium radical. Such radicals are weakly bound[9] and undergo facile cleavages of the C−N and N−H bonds, as examined in detail by neutralization−reionization mass spectrometry (NRMS)[10] for several model systems.[11] Cleavage of the N−H bond in the transient hypervalent radical releases a hydrogen atom that can be captured by an unsaturated group such as the amide carbonyl to form a transient amino(hydroxy)alkyl radical (Scheme 1). These transient intermediates may dissociate by cleavage of the adjacent N−C bonds, resulting in backbone fragmentations that provide sequence information about the ion.

Although reaction mechanisms have been proposed for ECD,[12] the complexity of the multiply charged peptide ions prevented detailed studies, and so the structure and energetics of the putative radical intermediates have been mostly speculative. Intramolecular hydrogen atom capture has been studied prior to ECD with model hexenyldimethylammonium[11g] or hexenylmethyloxonium radicals that contained a hypervalent ammonium or oxonium group, respectively, as an H atom donor and a carbon−carbon double bond as an H atom acceptor.[13] The donor and acceptor groups were positioned to sterically allow or prevent intramolecular H atom transfer, which was found to occur in the hypervalent oxonium radicals[13] but not in the ammonium radicals.[11g]

Recently, we have reported on radical intermediates pertinent to hydrogen atom adducts to the disulfide bond, which are also thought to play a role in ECD.[14] In the work reported here, we generated the amino(hydroxy)methyl radical (**1**) which is the prototypical hydrogen atom adduct to the amide bond. In addition to being a model for ECD, radical **1** belongs to the class of alkyl radicals carrying electron-donating substituents that have been of keen interest to experimental[15] and computational chemists.[16]

To generate radical **1**, we employ collisional electron transfer from a polarizable thermal donor, such as dimethyl disulfide or trimethylamine, to fast stable cation $\mathbf{1}^+$ (Scheme 2). It is well-established that charge transfer collisions with polarizable electron donors, even though occurring at high (kiloelectronvolt) translational energies, result in low to moderate vibrational excitation in the nascent neutral species, allowing for generation of even weakly bound radicals.[17]

Since the electron transfer occurs with impact parameters on the order of several molecular diameters (5−10 Å), an encounter of a thermal donor with a fast ion, such as $\mathbf{1}^+$ that travels at 186 000 m/s at 8250 eV, lasts only 3−5 fs. Hence, the transition from the ion potential energy surface to that of the radical is essentially a vertical process.[10b] Unimolecular dissociations of **1** are studied using variable-time neutralization−reionization

10.1021/jp012931i CCC: $20.00

**SCHEME 1**

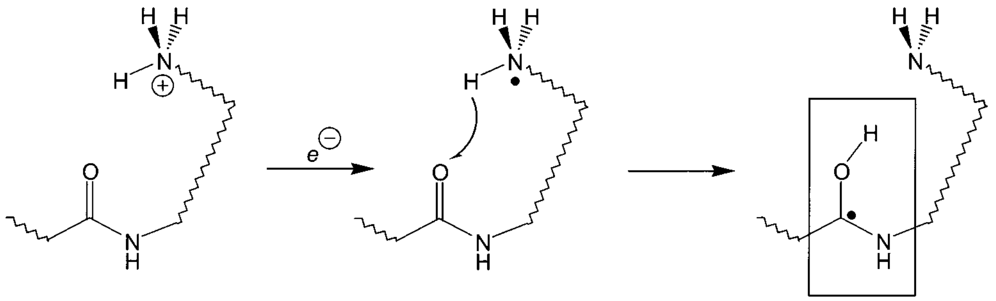

**SCHEME 2**

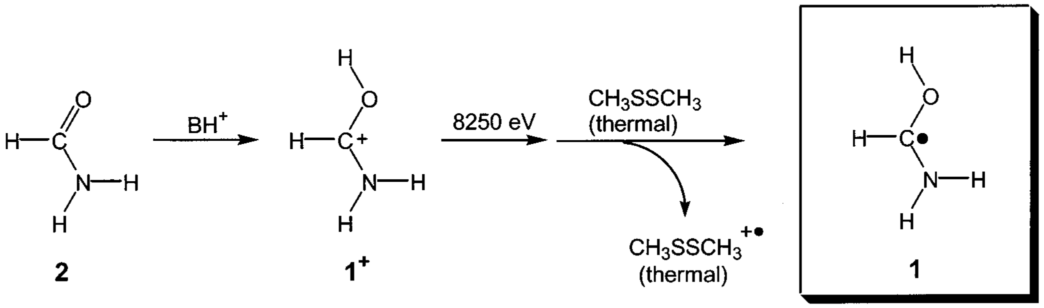

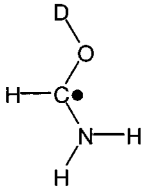

**1a**

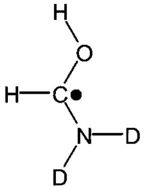

**1b**

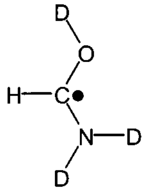

**1c**

mass spectrometry[18] in combination with isotope labeling. Variable-time measurements use temporal profiles of NR ion intensities to deconvolute unimolecular dissociations of neutral species produced by collisional neutralization from those of ions formed by collisional reionization, and also provide average rate parameters that quantify the contributions of neutral and ion processes.[18] High-level ab initio calculations are performed to provide relative and activation energies that are used for RRKM calculations of dissociation rate constants.

## Experimental Section

**Materials.** Formamide (**2**) (Baker), acetone (Fisher, 99.6%), dimethyl disulfide (DMDS, Aldrich), and trimethylamine (TMA, Matheson) were used as received. Deuterium-labeled reagents $D_2O$ and acetone-$d_6$ (both from Cambridge Isotope Laboratories, 99.9% D) were also used as received.

**[*N*-$D_2$]Formamide (2a).** Formamide (1 mL, 25 mmol) was stirred in $D_2O$ (2 × 10 mL) at room temperature for 5 min, and the solvent was evaporated in vacuo.

**Methods.** Measurements were performed on a tandem quadrupole acceleration−deceleration mass spectrometer described previously.[19] Cations $\mathbf{1}^+$−$\mathbf{1c}^+$ were generated in a tight chemical ionization (CI) source via selective protonation or deuteronation at O of **2** or **2a** using acetone or acetone-$d_6$, respectively, as the CI reagent gas at pressures of $0.6-2.2 \times 10^{-4}$ Torr as read on an ionization gauge. Typical ionization conditions were as follows: electron energy, 100 eV; emission current, 1 mA; and temperature, 215−250 °C. Cation radical $\mathbf{2}^{+\bullet}$ was generated in a standard electron ionization (EI) source. Typical ionization conditions were as follows: electron energy, 70 eV; emission current, 500 $\mu$A; and temperature, 265 °C. Stable precursor ions were passed through a quadrupole mass filter operated in the radio frequency-only mode, accelerated to a total kinetic energy of 8250 eV, and neutralized in the collision cell floated at −8170 V. Dimethyl disulfide (DMDS) or trimethylamine (TMA) was introduced into the differentially pumped collision cell at a pressure that resulted in 70% transmittance of the precursor ion beam. The ions and neutrals were allowed to drift to a four-segment conduit,[10c] where the ions were reflected by the first segment floated at 250 V. The neutral flight times in standard neutralization−reionization mass spectrometry (NRMS) measurements were 3.2 $\mu$s. The fast neutral species were reionized in the second collision cell with oxygen at a pressure that resulted in 70% transmittance of the precursor ion beam. The ions formed in the second collision cell were decelerated; the fast neutrals were blocked by a chicane lens[19] that also provided an ion kinetic energy filter, and the ions passing the filter were analyzed by a second quadrupole mass filter operated at unit mass resolution. The instrument was tuned daily to maximize the ion current of reionized $CS_2^{+\bullet}$. Typical spectra consisted of 30−50 accumulated repetitive scans. Variable-time measurements were performed as described previously.[18] The neutral flight times used to evaluate the unimolecular dissociation kinetics of **1** were 0.34, 0.95, and 1.55 $\mu$s.

Collisionally activated dissociation (CAD) spectra were measured on a JEOL HX-110 double-focusing mass spectrometer of forward geometry (the electrostatic sector E precedes the magnet B). Collisions with air were monitored in the first field-free region at a pressure that resulted in 70% transmittance of the ion beam at 10 keV. The spectra were obtained by scanning E and B simultaneously while maintaining a constant B/E ratio (B/E-linked scan).

**Calculations.** Standard ab initio and density functional theory calculations were performed using the Gaussian 98 suite of programs.[21] Geometries were initially optimized using Becke's hybrid functional (B3LYP)[22] and the 6-31+G(d,p) basis set, and reoptimized at either 6-311+G(2d,p) (for bound structures) or 6-311++G(2d,p) (for transition state structures). Some structures were additionally optimized at 6-31+G(d,p) using second-order perturbational Møller−Plesset calculations[23] employing excitations of all electrons, MP2(FULL). Spin-unrestricted calculations [UB3LYP and UMP2(FULL)] were used for open-shell systems. In the UB3LYP and UMP2(FULL) calculations, $\langle S^2 \rangle$ operator expectation values ranged from 0.75 to 0.76 and from 0.75 to 0.79 for local minima and transition state structures, respectively, indicating minimal spin contamination. Optimized structures were characterized by harmonic frequency analysis as local minima (all frequencies real) or first-order saddle points (one imaginary frequency). Zero-point vibrational energies (ZPVEs) were calculated from B3LYP/6-311+G(2d,p) and B3LYP/6-311++G(2d,p) frequencies, as well as MP2(FULL)/6-31+G(d,p) frequencies, which were scaled by 0.963 (ref 24; for other scaling factors, see ref 25) and 0.931, respectively. The rigid-rotor harmonic oscillator approximation was used in all thermochemical calculations. Single-point energies were calculated at several levels of theory. Composite G2(MP2) energies[26] were determined for all structures and transition states from MP2/6-311+G(3df,2p) and quadratic configuration interaction calculations, QCISD(T)/6-311G(d,p).[27] MP4(SDTQ) energies were calculated using an expanding basis set [6-311G(d,p), 6-311+G(d,p), 6-311G(2df,p)] and used to determine G2 energies[28] for several radicals, cations, and transition states of interest. In addition, coupled-cluster single-point energies[29,30] were obtained for selected structures using Dunning's correlation-consistent triple-ζ basis set augmented with diffuse functions on all atoms, CCSD(T)/aug-cc-pVTZ.[31] Spin contamination in the UMP2, UMP4(SDTQ), UQCISD(T), and UCCSD(T) calculations was small for local minima, as shown by spin expectation values $\langle S^2 \rangle$ that ranged from 0.75 to 0.76. However, $\langle S^2 \rangle$ values ranged from 0.75 to 0.94 for transition states. Spin annihilation using Schlegel's projection method[32] (PMP2)[21] reduced the $\langle S^2 \rangle$ values to $\leq 0.753$ for all structures.

Franck−Condon energies in vertical neutralization and reionization were taken as absolute differences between the total G2 energies of fully optimized ion or neutral structures and those in which an electron has been added to an optimized cation structure or subtracted from an optimized neutral structure. No zero-point corrections were applied to the calculated Franck−Condon energies.

Gradient optimizations of excited state geometries were performed with spin-unrestricted configuration interaction singles (UCIS)[33] using the 6-311+G(2d,p) basis set. Single-point energies were obtained from time-dependent density functional theory[34] calculations using the B3LYP hybrid functional and the 6-311++G(3df,2p) basis set.

RRKM calculations used Hase's program[35] that was recompiled for MS-DOS and run under Windows NT.[36] Vibrational state densities were obtained by a direct count of quantum states in 2 kJ/mol steps for internal energies up to 190−320 kJ/mol above the threshold. The rotational states were treated adiabatically,[37] and the microscopic rate constants [$k(E,J,K)$] were Boltzmann-averaged over the thermal distribution of rotational $J$ and $K$ states pertaining to the ion source temperature. Thermal rate constants were calculated using the standard transition state theory formulas.[38]

**TABLE 1: Collisionally Activated Dissociation Spectra of Ions 1$^+$−1c$^+$**

| | relative intensity[a] | | | | | relative intensity[a] | | | |
|---|---|---|---|---|---|---|---|---|---|
| *m/z* | **1**$^+$ | **1a**$^+$ | **1b**$^+$ | **1c**$^+$ | *m/z* | **1**$^+$ | **1a**$^+$ | **1b**$^+$ | **1c**$^+$ |
| 48 | − | − | − | 18.8[b] | 26 | − | 3.1 | − | − |
| 47 | − | − | 15.6[b] | 8.6 | 24 | − | 1.5 | 8.3 | − |
| 46 | − | 25.3[b] | 10.6 | 10.8 | 23 | 8.5 | 1.5 | − | − |
| 45 | 18.6 | 8.5 | 6.4 | − | 21 | − | − | − | 4.0 |
| 44 | 11.6 | 3.8 | 4.4 | 3.4 | 20 | − | − | 4.9 | 3.3 |
| 43 | 6.1[b] | 3.1 | 3.4 | − | 19 | − | 2.6 | 6.7 | 4.0 |
| 42 | − | 1.5 | − | − | 18 | 3.9 | 4.2 | 4.5 | 3.8 |
| 31 | − | 2.3 | 6.3 | 7.8 | 17 | 6.8 | 2.7 | − | − |
| 30 | 3.2 | 4.8 | 6.1 | 6.4 | 16 | 3.9 | 5.9 | − | − |
| 29 | 14.2 | 6.4 | 13.4 | 15.7 | 14 | − | 3.0 | − | − |
| 28 | 18.2 | 10.3 | 6.2 | 5.4 | 12 | − | 2.2 | − | − |
| 27 | 5.0 | 2.8 | − | − | | | | | |

[a] Relative to the sum of CAD ion intensities. [b] Dominant product of metastable ion dissociations.

## Results and Discussion

**Formation and Dissociations of the Amino(hydroxy)methyl Radical.** Radical **1** was generated via selective protonation of **2** followed by collisional electron transfer (Scheme 2). From G2 calculations of the topical proton affinities (PA) in **2**, it followed that protonation should be greatly preferred at the oxygen atom. Formation of the more stable conformer *anti*-**1**$^+$ was calculated to have a reaction enthalpy $-\Delta H_{\mathrm{r},298}$ (=PA) of 833 kJ/mol, whereas formation of *syn*-**1**$^+$ had a $-\Delta H_{\mathrm{r},298}$ of 820 kJ/mol. The ion structures and energies are discussed later in the paper. The calculated reaction enthalpies were in satisfactory agreement with the experimental proton affinity of formamide (822 kJ/mol).[39] Protonation at the nitrogen atom was calculated to be substantially less favorable, with a PA of 765 kJ/mol. Selective, mildly exothermic gas phase protonation of **2** and **2a** to form cations **1**$^+$ and **1a**$^+$, respectively, was therefore possible with $(CH_3)_2C{=}OH^+$ {PA[$(CH_3)_2C{=}O$] = 812 kJ/mol}.[39] Similarly, **2** and **2a** were selectively deuteronated with $(CD_3)_2C{=}OD^+$ to generate cations **1b**$^+$ and **1c**$^+$, respectively.[20] Ions **1**$^+$−**1c**$^+$ were characterized by CAD mass spectra which showed eliminations of H, $H_2$, $NH_3$, and $H_2O$ as the major ion dissociations (Table 1).

Collisional neutralization of **1**$^+$ yielded a substantial fraction of stable radicals which were detected following reionization as survivor ions at *m/z* 46 in the neutralization−reionization (NR) mass spectrum (Figure 1). Upon NR, the primary dissociations were loss of H (*m/z* 45) and rearrangements producing $NH_3^{+\bullet}$ and $OH^+$ (*m/z* 17) and $H_2O^{+\bullet}$ and $NH_4^+$ (*m/z* 18), with complementary fragments of the $CH_{0-1}O$ group (*m/z* 28−29) and $CH_{0-2}N$ group (*m/z* 26−28).

Deuterium labeling was employed to elucidate dissociation mechanisms, specifically for loss of hydrogen which was the dissociation of interest. NR of the O-D-labeled ion **1a**$^+$ showed an approximately 40% loss of a light hydrogen, with loss of deuterium overlapping with elimination of an $H_2$ molecule. The N-$D_2$-labeled ion **1b**$^+$ underwent an approximately 65% loss of light hydrogen and a 35% loss of D or $H_2$. As shown in the NR spectrum of the O,N-$D_3$-labeled ion **1c**$^+$, loss of hydrogen from C was negligible (∼5−10%) as compared to loss of deuterium. This led us to conclude that loss of hydrogen upon

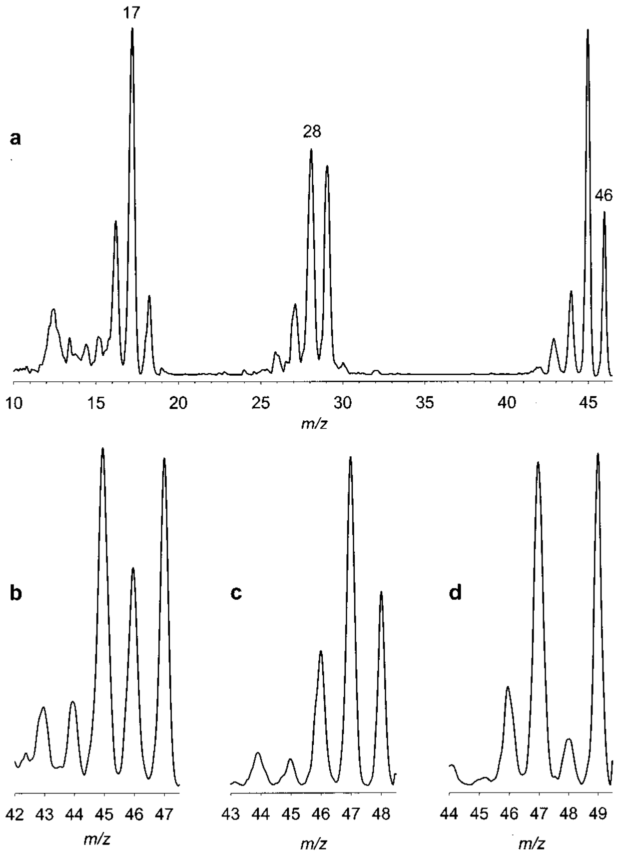

**Figure 1.** Neutralization (TMA, 70% transmittance)−reionization ($O_2$, 70% transmittance) mass spectra of (a) $\mathbf{1}^+$, (b) $\mathbf{1a}^+$, (c) $\mathbf{1b}^+$, and (d) $\mathbf{1c}^+$.

**TABLE 2: Ion Relative Energies**

| species/reaction | relative energy[a] G2(MP2)[b] |
|---|---|
| *anti*-$\mathbf{1}^+$ | 0 |
| *syn*-$\mathbf{1}^+$ | 13.4 |
| *anti*-$\mathbf{1}^+$ (VI)[c] | 136 |
| *syn*-$\mathbf{1}^+$ (VI)[c] | 150 |
| *anti*-$\mathbf{1}^+ \rightarrow \mathbf{2}^{+\bullet} + H^\bullet$ | 492 |
| *syn*-$\mathbf{1}^+ \rightarrow \mathbf{2}^{+\bullet} + H^\bullet$ | 478 |
| *anti*-$\mathbf{1}^+ \rightarrow \mathbf{3}^{+\bullet} + H^\bullet$ | 471.5 |
| *syn*-$\mathbf{1}^+ \rightarrow \mathbf{3}^{+\bullet} + H^\bullet$ | 484 |
| *anti*-$\mathbf{1}^+ \rightarrow \mathbf{4}^{+\bullet} + H^\bullet$ | 540 |
| *syn*-$\mathbf{1}^+ \rightarrow \mathbf{4}^{+\bullet} + H^\bullet$ | 528 |
| *anti*-$\mathbf{1}^+ \rightarrow \mathbf{2} + H^+$ | 826 (833)[d] |
| *syn*-$\mathbf{1}^+ \rightarrow \mathbf{2} + H^+$ | 813 (820)[d] |
| $O{=}CHNH_3^+ \rightarrow \mathbf{2} + H^+$ | 760 (765)[d] |
| *anti*-$\mathbf{1}^+ \rightarrow \mathbf{4} + H^+$ | 890 |
| *syn*-$\mathbf{1}^+ \rightarrow \mathbf{4} + H^+$ | 861 |
| *anti*-$\mathbf{1}^+ \rightarrow HC{=}O^+ + NH_3$ | 264 |
| *syn*-$\mathbf{1}^+ \rightarrow HC{=}O^+ + NH_3$ | 250 |
| *anti*-$\mathbf{1}^+ \rightarrow HC{=}NH^+ + H_2O$ | 188 |
| *syn*-$\mathbf{1}^+ \rightarrow HC{=}NH^+ + H_2O$ | 175 |

[a] In units of kilojoules per mole at 0 K. [b] From spin-projected MP2 energies wherever it applies. [c] Energy difference in kilojoules per mole between the vertically ionized cation and the optimized cation structure. [d] Topical proton affinities of **2**, at 298 K.

**TABLE 3: Rate Parameters for Neutral ($k_N$) and Ionic ($k_i$) Losses of H and D upon NR of $\mathbf{1a}^+$−$\mathbf{1c}^+$ [a]**

| | $\mathbf{1a}^+$ | $\mathbf{1b}^+$ | $\mathbf{1c}^+$ | | $\mathbf{1a}^+$ | $\mathbf{1b}^+$ | $\mathbf{1c}^+$ |
|---|---|---|---|---|---|---|---|
| $k_N$(H) | 0.22 | 0.31 | 0.082 | $k_i$(H) | 0.091 | 0.58 | – |
| $k_N$(D) | 0.37 | 0.10 | 0.28 | $k_i$(D) | 0.30 | 0.67 | 0.14 |

[a] $10^6\ s^{-1}$.

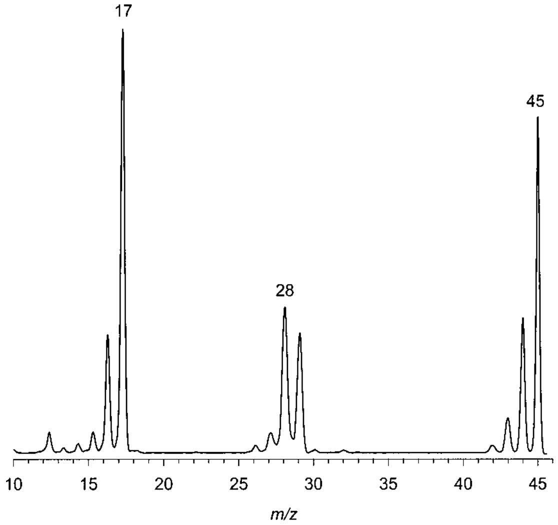

**Figure 2.** Neutralization ($CH_3SSCH_3$, 70% transmittance)−reionization ($O_2$, 70% transmittance) mass spectrum of $\mathbf{2}^{+\bullet}$.

NR of $\mathbf{1}^+$ occurs in an approximately 4:1 ratio from O versus N. However, because reionization is necessary for mass analysis of neutral precursors and dissociation products, NR spectra consist of overlapping neutral and post-reionization ion dissociations. Deconvolution of these dissociations was accomplished by variable-time measurements combined with deuterium labeling and by identifying purely ion dissociations from CAD spectra of isotopomers $\mathbf{1a}^+$−$\mathbf{1c}^+$ (Table 1).

The latter spectra showed predominant (70%) loss of the H atom from C ($\mathbf{1c}^+$, Table 1), while loss of the N−H (5%) and O−H (25%) hydrogen atoms was less abundant. The branching ratios for the ion dissociations qualitatively agreed with product ion relative stabilities. The amino(hydroxy)carbene cation radical ($\mathbf{3}^{+\bullet}$), which was formed by loss of the H−C hydrogen atom, was calculated to be the most stable isomer (vide infra), followed by $\mathbf{2}^{+\bullet}$ and [hydroxymethylenimine]$^{+\bullet}$ ($\mathbf{4}^{+\bullet}$, Table 2), in keeping with previous computational studies.[40,41] Hence, the CAD spectra combined with deuterium labeling showed that ion dissociations had mechanisms distinctly different from those observed upon NR.

Further distinction of neutral and post-reionization dissociations was obtained from variable-time NR measurements, which provided rate parameters that allowed us to quantify the relative contributions of neutral ($k_N$) and ion ($k_i$) bond cleavages to the total loss of H and (D/$H_2$). Although losses of $H_2$ and D were not resolved experimentally, the dissociation energetics disfavor both concerted and stepwise elimination of $H_2$, as discussed below. The rate parameters were measured by monitoring the [C,(H,D)$_3$,N,O]$^{+\bullet}$ channels in the variable-time spectra. The $H^+$/$D^+$ channels were not monitored because of the very small kinetic energies of these light fragments that resulted in substantial transmission losses. The rate parameters for neutral and ionic losses of H and D following NR of $\mathbf{1a}^+$−$\mathbf{1c}^+$ are summarized in Table 3. The data showed the preferential loss of the hydrogen atom from the OH group in **1** and a very small contribution of the loss of H from the C−H group. The reaction mechanisms leading to competitive losses from **1** of chemically different hydrogen atoms will be discussed below together with the dissociation energetics.

A reference NR spectrum of formamide (**2**) was obtained to help identify primary and consecutive dissociations of radical **1**. The NR spectrum of **2** (Figure 2) displayed dissociation products that were quite similar to those found in the NR spectrum of radical **1** (Figure 1a). This indicated, in line with the results from the variable-time spectra, that radical **1**

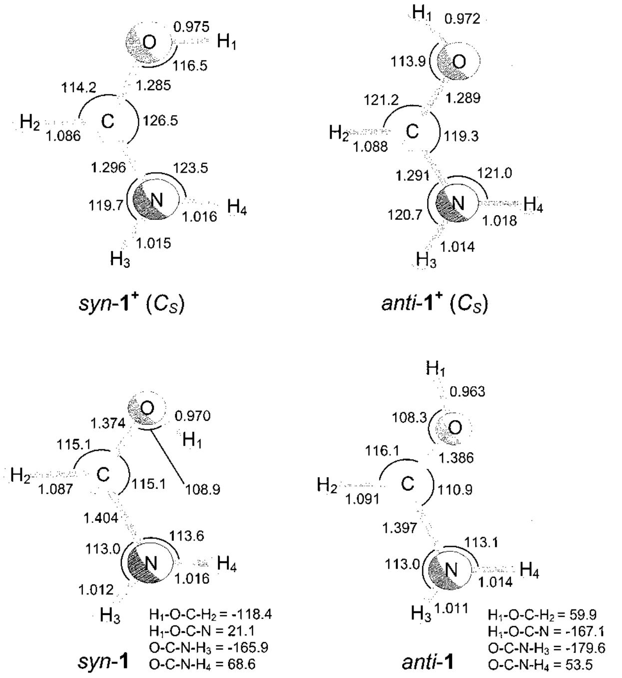

**Figure 3.** B3LYP/6-311+G(2d,p)-optimized structures of *syn*- and *anti*-$\mathbf{1}^+$ and -**1**. Bond lengths are in angstroms, and bond and dihedral angles are in degrees.

dissociated mainly by loss of H to form **2** which underwent consecutive dissociations. Because **2** is a substantially stable molecule, it is reasonable to assume that its NR dissociations occurred mostly after collisional ionization and were governed by ion dissociation mechanisms. This is corroborated by the CAD spectrum of $\mathbf{2}^{+\bullet}$ reported previously,[42] which showed dissociations similar to those in Figure 2. Interestingly, the *m*/*z* 45:*m*/*z* 17 ratio was larger for NR of **1** than for **2**, indicating that the [C,$H_3$,N,O] molecules resulting from loss of H from **1** were less energetic than the formamide molecule produced by neutralization of $\mathbf{2}^{+\bullet}$. The energetics of ion and radical dissociations were addressed with ab initio calculations, as discussed next.

**Ion and Radical Energetics.** Two local energy minima for both cation $\mathbf{1}^+$ and radical **1** were found by high-level ab initio calculations (Figure 3). At G2, the isomer with an outward (*anti*) orientation of the O−H bond (*anti*-$\mathbf{1}^+$) was 13.4 kJ/mol more stable than the *syn* rotamer (*syn*-$\mathbf{1}^+$). Radical **1** exhibited a weaker preference for the *anti* rotamer (*anti*-**1**) which was only 0.7 kJ/mol more stable than the *syn* rotamer (*syn*-**1**). From the calculated entropy, enthalpy, electronic, and zero-point vibrational energy contributions, Gibbs free energies and equilibrium constants were determined for the rotational equilibrium between the *syn* and *anti* rotamers for both cation $\mathbf{1}^+$ and radical **1**. At temperatures between 473 and 573 K (the typical working temperature range of the ion source), $\mathbf{1}^+$ was calculated to exist as 94−97% *anti*-$\mathbf{1}^+$ while radical **1** was approximately 55−58% *anti*-**1**. Transition state energies for the rotation about the C−O bond were calculated at the G2 level of theory as 5 and 50 kJ/mol for **1** and $\mathbf{1}^+$, respectively, relative to the corresponding more stable *anti* rotamers. This indicated that *anti*−*syn* interconversion was both thermodynamically and kinetically disfavored in ions $\mathbf{1}^+$, but extremely facile in radical **1**. A similar relationship has been found previously for the torsional barriers in the hydroxymethyl cation and radical.[43]

Franck−Condon energies were calculated by G2 for the vertical neutralization of $\mathbf{1}^+$ to **1** as 82 kJ/mol for *anti*-$\mathbf{1}^+$ → *anti*-**1**, and 92 kJ/mol for *syn*-$\mathbf{1}^+$ → *syn*-**1**. This pointed to substantial vibrational excitation in the ground electronic state ($^2X$) of **1** formed by vertical electron capture.

**Dissociation Energetics.** Transition states for the loss of hydrogen from both O and N in **1** were determined at several levels of theory (Figure 4). Potential energy surfaces (PESs) along the dissociation coordinates were investigated with UB3LYP/6-311++G(2d,p) and UMP2/6-31+G(d,p) for reaction pathways for O−H and N−H cleavages in which the corresponding bonds were stretched by 0.02 Å increments while the remaining internal degrees of freedom were fully optimized (Figure 5). For either bond cleavage starting from *syn*-**1**, UMP2 calculations produced a discontinuous PES with cusps at 1.3 Å along the O−H coordinate and at 1.53 Å for the N−H coordinate. In contrast, smooth energy surfaces with first-order saddle points were obtained by UB3LYP. The connectivity of the reactants and transition states was confirmed by intrinsic reaction coordinate calculations.[44] The points on the UB3LYP PES were then treated with G2(MP2) and G2 single-point calculations that provided corrected PES profiles along the reaction coordinates. These showed significant shortening of the transition state bond lengths from the UB3LYP-optimized saddle points that was practically identical for G2(MP2) and G2. For example, the O−H bond dissociation (**TS1**) showed G2(MP2) and G2 transition states at a *d*(O−H) of 1.38 Å compared with a value of 1.44 Å from the UB3LYP saddle point, and the N−H dissociations exhibited a shortening from 1.76 to 1.6 Å in **TS2** and from 1.78 to 1.62 Å in **TS3**. Regardless of the *syn* or *anti* reactant radical geometry, O−H dissociations starting from both rotamers converged to the same transition state (**TS1**), which was 98 kJ/mol above *anti*-**1** as determined by G2(MP2). In contrast, distinct transition states were found for cleavages of the N−H bonds, e.g., 116 kJ/mol from *syn*-**1** (**TS2**) and 130 kJ/mol from *anti*-**1** (**TS3**), both energies determined by G2(MP2). The G2(MP2) and/or G2 potential energy surfaces were fitted with polynomials, and the saddle points along the corresponding O−H and N−H coordinates were used for G2 and CCSD(T)/aug-cc-pVTZ single-point energy calculations. The pertinent relative energies are summarized in Figure 6.

The PES for a concerted elimination of $H_2$ from *anti*-**1** was investigated by UB3LYP calculations. The potential energy showed a sharp increase upon bringing the C−H and O−H hydrogen atoms together in an attempt to achieve a four-membered transition state. At H−H distances of 0.92−0.9 Å, the PES exhibited a very high energy (>300 kJ/mol above *anti*-**1**) and negative curvatures along two internal coordinates. Upon further H···H approach, the system collapsed to the transition state for H atom abstraction (**TS8**; see below). This indicated that there was not a true transition state for a concerted elimination of an $H_2$ molecule from *anti*-**1**.

In addition, since the loss of the hydroxyl H atom has a substantial reverse activation barrier [e.g., 51 kJ/mol by CCSD(T), Table 4], the departing hydrogen atom gains kinetic energy and recoils from **2**. Hence, under low-pressure conditions, the departing H atom cannot return to engage in an exothermic abstraction of the methine hydrogen to form $H_2$. These constraints argue strongly against unimolecular elimination of $H_2$ from *anti*-**1**.

Three other [C,$H_4$,N,O] isomers with the N−C−O frame were found to be local energy minima (Figure 7) that were connected to *syn*- and *anti*-**1** by transition states for isomerizations (**TS4**−**TS7**, Figure 4). These isomers were potential intermediates for hydrogen atom scrambling by migrations between C, N, and O. The *anti* and *syn* hydroxymethylamidyl radicals (*anti*-**5** and

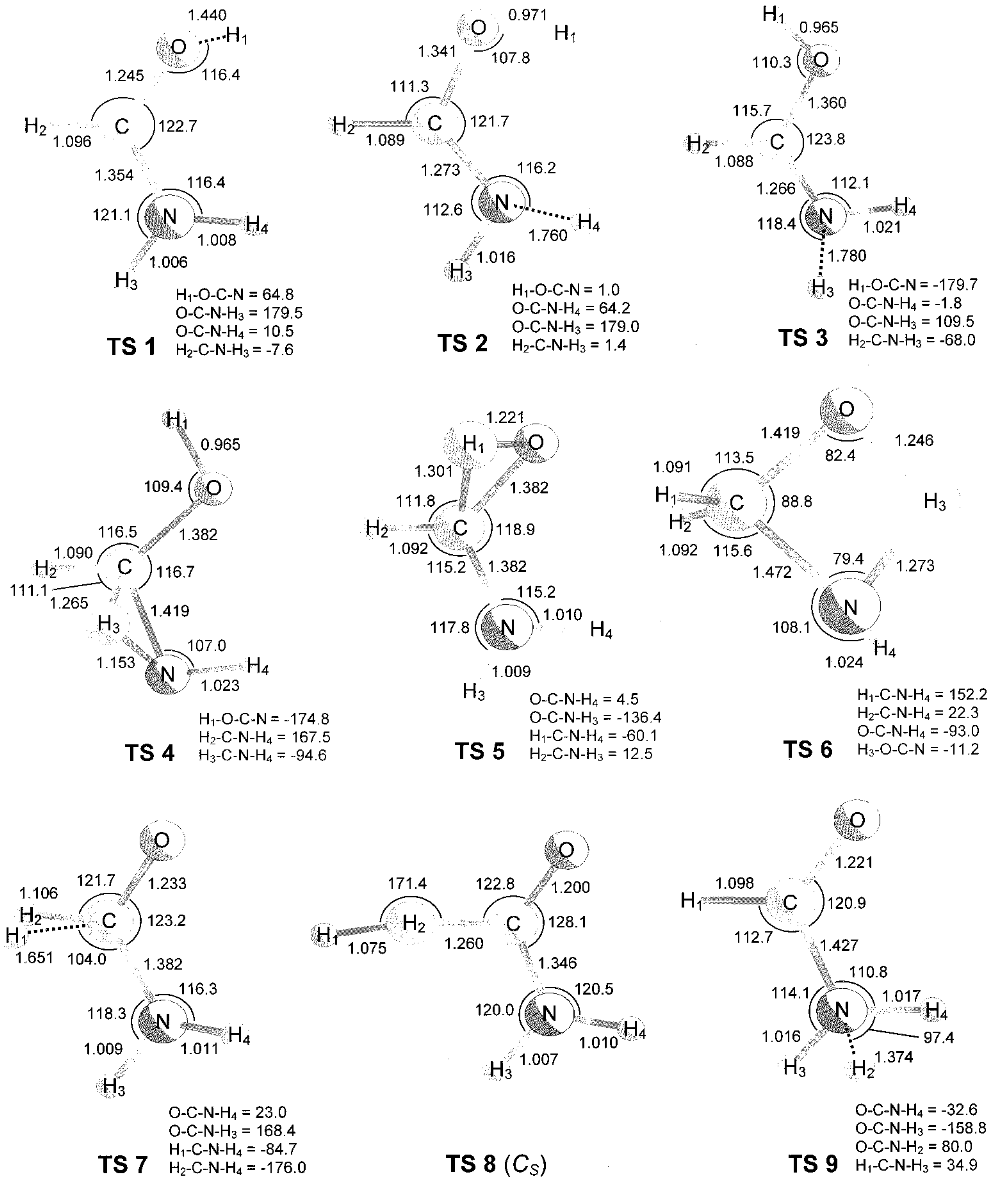

**Figure 4.** B3LYP/6-311++G(2d,p)-optimized structures of **TS1-TS3** and B3LYP/6-311+G(2d,p) optimized structures of **TS4-TS9**.

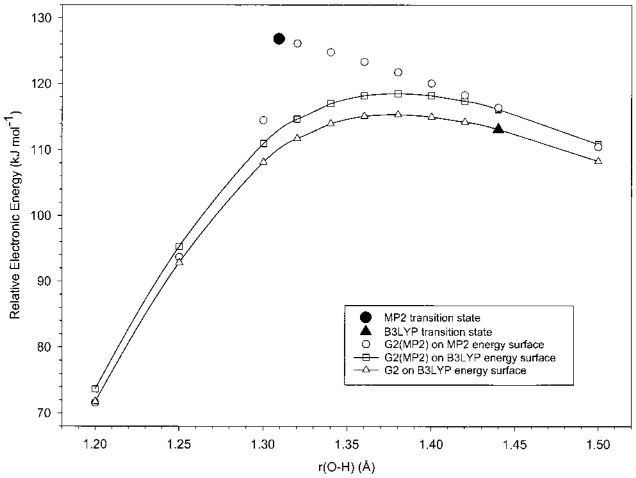

**Figure 5.** Potential energy profile along the O−H coordinate in dissociation of **1**.

*syn*-**5**, respectively) were 30 and 25 kJ/mol less stable than *anti*-**1**. The aminomethyloxy radical (**6**) was 51 kJ/mol less stable than *anti*-**1** (Table 4). These relative stabilities closely follow the order of typical bond dissociation energies: BDE(O−H) > BDE(N−H) > BDE($C_{sp3}$−H).[45]

Transition state geometries were obtained for *anti*-**1** → *anti*-**5** (**TS4**), *anti*-**1** → **6** (**TS5**), and *syn*-**5** → **6** (**TS6**) isomerizations (Figure 6). However, the corresponding transition state energies were ≥50 kJ/mol above that for **TS1** (Table 4). This indicated that *anti*-**1** should dissociate selectively through the lowest-energy channel without undergoing isomerizations that would scramble the nonequivalent hydrogen atoms. Interestingly, according to CCSD(T) calculations, dissociation of one of the C−H bonds in **6** was 2 kJ/mol exothermic but required a 47 kJ/mol transition state (**TS7**) to produce **2** and a hydrogen atom. However, isomer **6** was energetically inaccessible from **1** on the ground ($^2X$) state PES.

To quantify the radical dissociations, we used the G2, G2(MP2), and CCSD(T) energy barriers and UB3LYP/6-311++G(2d,p) harmonic frequencies and moments of inertia to calculate RRKM rate constants. The results of these calculations are shown in Figure 8 for transition states on the CCSD(T)-calculated PES of *syn*-**1**. Not surprisingly, the *anti*-**1** ↔ *syn*-**1** interconversion was several orders of magnitude faster than bond dissociations at near-barrier internal energies. Hence, the transi-

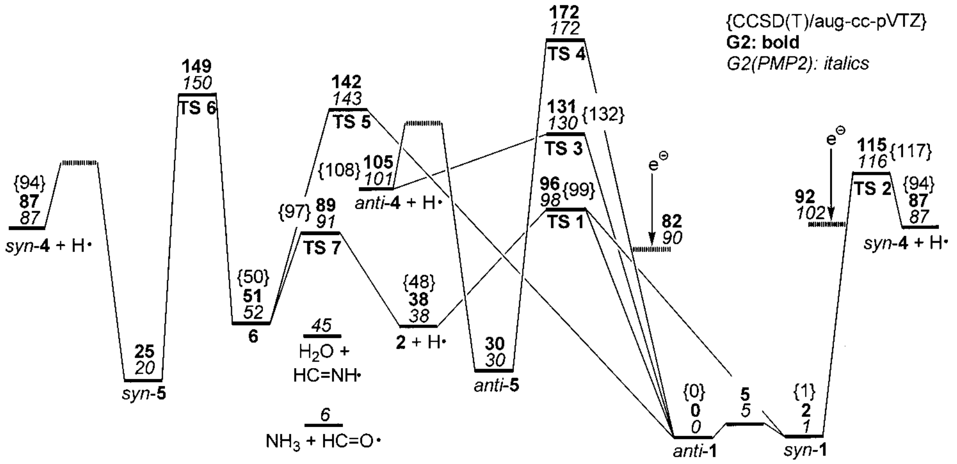

**Figure 6.** Potential energy diagram for dissociations of **1**.

**TABLE 4: Radical Relative Energies**

| | relative energy[a] | | |
|---|---|---|---|
| species/reaction | G2(MP2)[b] | G2[b] | CCSD(T)/ aug-cc-pVTZ |
| *anti*-**1** | 0 | 0 | 0 |
| *syn*-**1** | 0.7 | 2.2 | 0.7 |
| *anti*-**1** (VN)[c] | 90 | 82 | – |
| *syn*-**1** (VN)[c] | 102 | 92 | – |
| *anti*-**1** → **2** + H• | 38 | 38 | 48 |
| *syn*-**1** → **2** + H• | 37 | 35 | 47 |
| *anti*-**1** → *anti*-**4** + H• | 10 | 105 | 108 |
| *syn*-**1** → *syn*-**4** + H• | 86 | 84.5 | 93 |
| *anti*-**1** → HC=O• + NH$_3$ | 6 | – | – |
| *syn*-**1** → HC=O• + NH$_3$ | 5 | – | – |
| *anti*-**1** → HC=NH• + H$_2$O | 45 | – | – |
| *syn*-**1** → HC=NH• + H$_2$O | 45 | – | – |
| *anti*-**1** → HCNH$_2$ + OH• | 289 | – | – |
| *syn*-**1** → HCNH$_2$ + OH• | 289 | – | – |
| *anti*-**5** | 30 | 30 | – |
| *syn*-**5** | 20 | 25 | – |
| **6** | 52 | 51 | – |
| **TS1** | 98 | 96 | 99 |
| **TS2** | 116 | 115 | 117 |
| **TS3** | 130 | 131 | 132 |
| **TS4** | 172.5 | 172 | – |
| **TS5** | 143 | 142 | – |
| **TS6** | 150 | 149 | – |
| **TS7** | 91 | 88.5 | – |

[a] In units of kilojoules per mole at 0 K. [b] From spin-projected MP2 energies wherever it applies. [c] Energy difference in kilojoules per mole between the vertically neutralized radical and the optimized neutral structure.

tion state for O−H bond dissociation, and the lower of the two N−H dissociation transition states (cf. Figure 6), are both accessible through *syn*-**1**, and so discussion of unimolecular rate constants will focus on processes starting from this rotamer.

The calculations clearly suggested that for the range of internal energies that was investigated (dissociation threshold to 320 kJ/mol), loss of H from **1** should occur predominantly from the OH group. Rate constants for O−H bond dissociation and rotamer interconversion, however, approach each other at very high internal energies (>300 kJ/mol). Unimolecular rate constants for O−H and N−H bond dissociations differed from each other by 1 order of magnitude at an internal energy of ~190 kJ/mol, and converged somewhat at higher energies.

**Dissociation Mechanisms.** In this section, we address two important questions concerning the nature of unimolecular dissociations of radical **1**. (1) What are the sources of internal energy that drive the dissociations of **1**? (2) How do the observed branching ratios compare with those predicted by RRKM calculations?

The internal energy of vertically formed **1** contains contributions from the internal energy of the precursor ion ($E_{\mathrm{ion}}$), the Franck−Condon energy gained upon electron transfer ($E_{\mathrm{FC}}$), and the excitation energy of the particular electronic state being formed ($\Delta E_{\mathrm{exc}}$). We have shown previously[46] that the most probable internal energy $\langle E_{\mathrm{int}}\rangle$ of radicals produced by NR in the ground electronic state ($\Delta E_{\mathrm{exc}} = 0$) can be expressed as a simple sum of two terms; e.g., $\langle E_{\mathrm{int}}\rangle = E_{\mathrm{ion}} + E_{\mathrm{FC}}$. Out of these, $E_{\mathrm{FC}}$ was obtained by G2 calculations as 82 kJ/mol. $E_{\mathrm{ion}}$ was estimated to be 37 kJ/mol from the thermal energy of **2** at the ion source temperature (20 kJ/mol at 523 K) and an ≈80% fraction of protonation exothermicity (17 kJ/mol).[47] These energy contributions were calculated for *anti*-**1**, as the precursor cation equilibrium is dominated by this isomer, as described above. From the energy terms for $E_{\mathrm{ion}}$ and $E_{\mathrm{FC}}$, one obtains an $\langle E_{\mathrm{int}}\rangle$ of 119 kJ/mol in *anti*-**1**. This is sufficient to drive dissociation of the O−H bond in *anti*-**1** which requires 96−99 kJ/mol in **TS1** at the present levels of theory. However, RRKM rate constants obtained for an $\langle E_{\mathrm{int}}\rangle$ of 119 kJ/mol predict branching ratios [$k$(O−H)/$k$(N−H)] for the dissociations of the O−H and N−H bonds in **1** to be >10 (Figure 8), which substantially exceeds the experimental value from variable-time measurements (1.7, Table 3). The experimental branching ratio can be approached at much higher internal energies of dissociating **1**, which, however, are not likely to be populated in the ground electronic state.

Another source of internal energy in vertically formed **1** can be provided by internal conversion from an excited electronic state. The corresponding excitation energies ($\Delta E_{\mathrm{exc}}$) and radiative lifetimes were calculated by time-dependent B3LYP for the five lowest excited states (*A*−*E*) of *syn*-**1** and *anti*-**1**, as summarized in Table 5. To be kinetically relevant, the excited states of **1** must have long radiative lifetimes ($\tau$) that are commensurate with the dissociation kinetics such that $\tau \approx 1/k$, where $k$ is the unimolecular rate constant for the dissociation in question. Table 5 shows that the lowest three excited electronic states of *syn*- and *anti*-**1** have microsecond radiative lifetimes due to dipole-forbidden radiative transitions to the *X* state.

The vertical and adiabatic excitation energies of the *A* and *B* states are shown in Figure 9. The vertical $\Delta E_{\mathrm{exc}}$ at the optimized geometry of the *A* state is only 0.17 eV from the *X* state potential energy surface, indicating a facile *A* → *X* internal conversion that can convert 1.43 eV (138 kJ/mol) of the adiabatic excitation

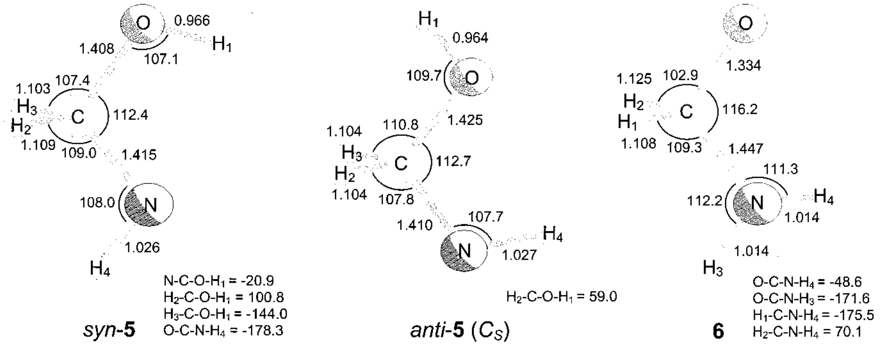

**Figure 7.** B3LYP/6-311+G(2d,p)-optimized structures of *syn*-**5**, *anti*-**5**, and **6**.

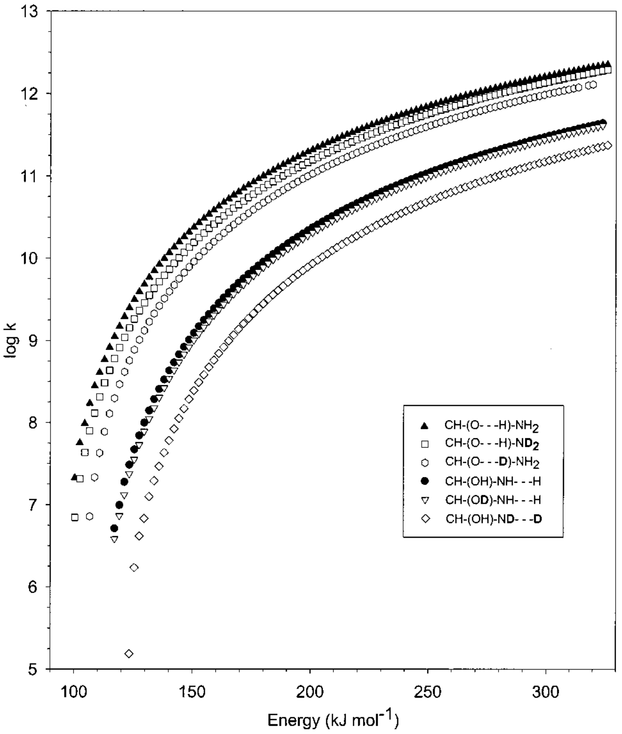

**Figure 8.** RRKM unimolecular rate constants (log, $s^{-1}$) for dissociations of *syn*-**1**.

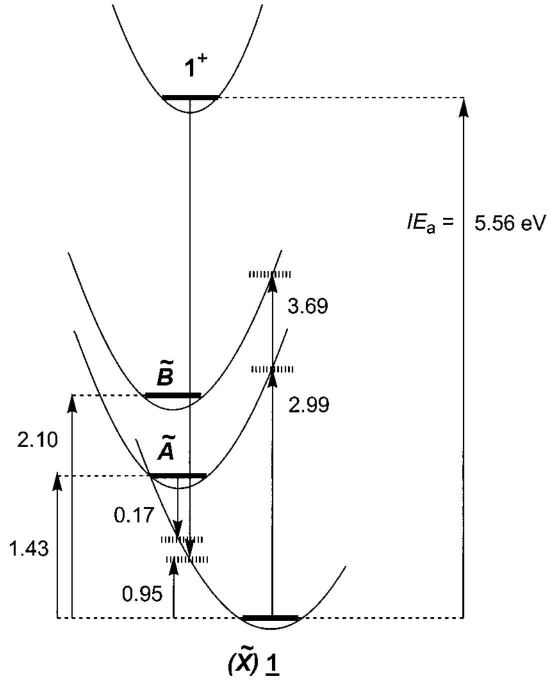

**Figure 9.** Excitation energies for the *A* and *B* states in **1**.

energy plus 37 kJ/mol of ion thermal energy into vibrational excitation of the *X* state. Likewise, internal conversion from the *B* state could provide ca. 240 kJ/mol of vibrational excitation in the *X* state. The RRKM calculations (Figure 8) indicate that $k > 10^{10}$ $s^{-1}$ at these internal energies of (*X*)**1**. That dissociations on the microsecond time scale are observed can be explained by a two-step process, in which a rate-determining internal conversion ($A \rightarrow X$, or $B \rightarrow X$) is followed by fast dissociation of the vibrationally excited *syn*,*anti*-**1** occurring on the ground state potential energy surface. Dissociations of highly excited **1** also allow for an improved but still not perfect fit of the experimental and RRKM branching ratios. For example, at $E_{int}$ values of 175 and 240 kJ/mol, RRKM calculations predicted *k*(O−D)/*k*(N−H) values of 6.4 and 4.2, respectively (including primary and secondary isotope effects), to be compared with 1.7 from experiment.

We also considered dissociations of **1** on the potential energy surface of an excited electronic state as a possible explanation for the competing O−H and N−H bond cleavages. Although we did not study the potential energy surfaces of the excited state *syn*-**1** in detail, some qualitative conclusions can be made with the data in hand. The first excited state of formamide enol (*syn*-**4**) was calculated to require an excitation energy $\Delta E_{exc}$ of 6.4 eV for the $X \rightarrow A$ transition, which corresponds to electron excitation from an in-plane $\pi_{xy}$ orbital to a $\pi_z$* orbital.[48] This put the energy of ($^1A$)*syn*-**4** + H$^•$ at 7.3 eV relative to **1** (*syn* or *anti*) which was substantially above the ionization energy of the radical [5.56 eV as determined by G2(MP2)]. Hence, the first excited state of *syn*-**4** was energetically inaccessible by dissociation of **1**. Similar conclusions followed from the analysis of excited electronic states of formamide (**2**).[49] The $^1A$ state of **2**, which is due to an electron transition from an in-plane $\pi_{xy}$ orbital to a $\pi_z$* orbital, was both measured[49] and calculated here[48] to be 5.6 eV above the ground state. Hence, the total energy of ($^1A$)**2** + H$^•$ is 6.0 eV relative to **1**, which is again well above the radical ionization energy. This simple analysis showed that loss of H from **1** to form dissociation products in excited electronic states was energetically impossible.

**Tunneling Effects.** Since the experimental branching ratios were obtained from competitive dissociations of O−D and N−H bonds, isotope effects on quantum mechanical tunneling through the corresponding energy barriers can become important in affecting the dissociation kinetics.[50] We used an asymmetrical Eckart barrier[51] as a model for the energy barriers involved with O−(H,D) and N−(H,D) bond cleavages. Barrier permeability, *G*, or the probability of appearing on the other side of the energy

**TABLE 5: Excited State Energies and Radiative Lifetimes of Radicals *syn*-1 and *anti*-1**

| radical-optimized geometry | state | $\Delta E$[a] | | $f$[b] | | $\tau$ ($\mu$s) | | configuration[c] | |
|---|---|---|---|---|---|---|---|---|---|
| | | CIS[d] | TD-B3LYP[e] | CIS | TD-B3LYP | CIS | TD-B3LYP | CIS | TD-B3LYP |
| (*X*) *syn*-1[f] | *A* | – | 2.99 | – | 0.004 | – | 0.6 | – | 13α−14α |
| | *B* | – | 3.69 | – | 0.015 | – | 0.1 | – | 13α−15α |
| | *C* | – | 3.87 | – | 0.009 | – | 0.2 | – | 13α−16α |
| | *D* | – | 4.53 | – | 0.028 | – | 0.04 | – | 13α−17α |
| | *E* | – | 5.33 | – | 0.024 | – | 0.03 | – | 13α−18α |
| (*X*) *anti*-**1**[f] | *A* | – | 2.82 | – | 0.003 | – | 0.9 | – | 13α−14α |
| | *B* | – | 3.28 | – | 0.004 | – | 0.6 | – | 13α−15α |
| | *C* | – | 3.70 | – | 0.005 | – | 0.3 | – | 13α−16α |
| | *D* | – | 4.54 | – | 0.002 | – | 0.7 | – | 13α−17α |
| | *E* | – | 4.70 | – | 0.050 | – | 0.02 | – | 13α−18α |
| (*A*) *syn*-**1**[g] | *A* | 1.85 | 0.17 | 0.000 | 0.000 | >20 | >20 | 13α−14α | 13α−14α |
| | *B* | 2.54 | 0.85 | 0.0035 | 0.0004 | 1.0 | >20 | 13α−15α | 13α−15α |
| | *C* | 3.15 | 1.32 | 0.0093 | 0.005 | 0.2 | 2.5 | 13α−16α | 13α−16α |
| | *D* | 3.48 | 2.18 | 0.0166 | 0.003 | 0.1 | 1.9 | 13α−17α | 13α−17α |
| | *E* | 4.61 | 2.29 | 0.0014 | 0.016 | 0.8 | 0.3 | mixed α | 13α−18α |
| (*A*) *anti*-**1**[g] | *A* | 1.71 | 0.17 | 0.0005 | 0.003 | 2.4 | >20 | 13α−14α | mixed α |
| | *B* | 2.52 | 0.81 | 0.0022 | 0.001 | 1.7 | >20 | 13α−15α | 13α−15α |
| | *C* | 2.96 | 1.29 | 0.0018 | 0.002 | 1.5 | 7.3 | 13α−16α | 13α−16α |
| | *D* | 3.33 | 2.16 | 0.0176 | 0.0165 | 0.1 | 0.3 | 13α−17α | 13α−18α |
| | *E* | 4.55 | 2.17 | 0.0163 | 0.0035 | 0.07 | 1.4 | 13α−18α | 13α−17α |
| (*B*) *syn*-**1**[g] | *A* | 1.87 | 0.16 | 0.000 | 0.0001 | >20 | >20 | 13α−14α | 13α−14α |
| | *B* | 2.39 | 0.78 | 0.0034 | 0.0005 | 1.2 | >20 | 13α−15α | 13α−15α |
| | *C* | 3.11 | 1.30 | 0.0092 | 0.0054 | 0.3 | 2.5 | 13α−16α | 13α−16α |
| | *D* | 3.44 | 2.17 | 0.0183 | 0.0023 | 0.1 | 2.1 | 13α−17α | 13α−17α |
| | *E* | 4.58 | 2.28 | 0.0006 | 0.0172 | 1.8 | 0.3 | mixed α | 13α−18α |
| (*B*) *anti*-**1**[g] | *A* | 1.94 | 0.41 | 0.0038 | 0.0009 | 1.6 | >20 | 13α−14α | 13α−14α |
| | *B* | 2.58 | 0.90 | 0.0032 | 0.0017 | 1.1 | 16.7 | 13α−15α | 13α−15α |
| | *C* | 3.08 | 1.40 | 0.0014 | 0.0017 | 1.7 | 6.9 | 13α−16α | 13α−16α |
| | *D* | 3.45 | 2.24 | 0.0201 | 0.0031 | 0.1 | 1.5 | 13α−17α | 13α−17α |
| | *E* | 4.64 | 2.29 | 0.0130 | 0.0188 | 0.08 | 0.2 | 13α−18α | 13α−18α |
| (*C*) *syn*-**1**[g] | *A* | 2.02 | 0.28 | 0.000 | 0.0001 | >20 | >20 | 13α−14α | 13α−14α |
| | *B* | 2.64 | 0.95 | 0.0042 | 0.0003 | 0.8 | >20 | 13α−15α | 13α−15α |
| | *C* | 3.13 | 1.29 | 0.0073 | 0.0047 | 0.3 | 2.9 | 13α−16α | 13α−16α |
| | *D* | 3.58 | 2.24 | 0.0173 | 0.0028 | 0.1 | 1.6 | 13α−17α | 13α−17α |
| | *E* | 4.74 | 2.38 | 0.0015 | 0.0164 | 0.7 | 0.2 | mixed α | 13α−18α |
| (*C*) *anti*-**1**[g] | *A* | 2.01 | 0.46 | 0.0039 | 0.0009 | 1.5 | >20 | 13α−14α | 13α−14α |
| | *B* | 2.70 | 1.00 | 0.0033 | 0.0016 | 1.0 | 14.3 | 13α−15α | 13α−15α |
| | *C* | 3.00 | 1.36 | 0.0018 | 0.0023 | 1.4 | 5.4 | 13α−16α | 13α−16α |
| | *D* | 3.48 | 2.28 | 0.0205 | 0.0026 | 0.02 | 0.09 | 13α−17α | 13α−17α |
| | *E* | 4.70 | 2.31 | 0.0110 | 0.0190 | 0.09 | 0.2 | 13α−18α | 13α−18α |
| (*D*) *syn*-**1**[g] | *A* | 1.88 | 0.20 | 0.000 | 0.0001 | >20 | >20 | 13α−14α | 13α−14α |
| | *B* | 2.50 | 0.87 | 0.0041 | 0.0005 | 0.9 | >20 | 13α−15α | 13α−15α |
| | *C* | 3.11 | 1.31 | 0.0089 | 0.0055 | 0.3 | 2.5 | 13α−16α | 13α−16α |
| | *D* | 3.43 | 2.19 | 0.0180 | 0.0024 | 0.1 | 2.0 | 13α−17α | 13α−17α |
| | *E* | 4.61 | 2.27 | 0.0016 | 0.0169 | 0.7 | 0.3 | mixed α | 13α−18α |
| (*D*) *anti*-**1**[g] | *A* | 1.85 | 0.33 | 0.0039 | 0.0008 | 1.7 | >20 | 13α−14α | 13α−14α |
| | *B* | 2.55 | 0.89 | 0.0032 | 0.0015 | 1.1 | 19.5 | 13α−15α | 13α−15α |
| | *C* | 2.95 | 1.32 | 0.0019 | 0.0021 | 1.4 | 6.3 | 13α−16α | 13α−16α |
| | *D* | 3.33 | 2.19 | 0.0200 | 0.0032 | 0.1 | 1.5 | 13α−17α | 13α−17α |
| | *E* | 4.57 | 2.19 | 0.0132 | 0.0186 | 0.08 | 0.3 | 13α−18α | 13α−18α |
| (*E*) *syn*-**1**[g] | *A* | 2.43 | 0.61 | 0.0003 | 0.0003 | 13.1 | >20 | 13α−14α | 13α−14α |
| | *B* | 3.30 | 1.38 | 0.0044 | 0.0002 | 0.5 | >20 | 13α−15α | 13α−15α |
| | *C* | 3.79 | 1.89 | 0.0101 | 0.0063 | 0.2 | 1.0 | 13α−16α | 13α−16α |
| | *D* | 4.07 | 2.34 | 0.0011 | 0.0013 | 1.3 | 3.2 | mixed α | 13α−17α |
| | *E* | 4.21 | 2.93 | 0.0204 | 0.0196 | 0.06 | 0.1 | 13α−17α | 13α−18α |
| (*E*) *anti*-**1**[g] | *A* | 2.00 | 0.37 | 0.0017 | 0.0002 | 3.4 | >20 | 13α−14α | 13α−14α |
| | *B* | 2.64 | 0.91 | 0.0072 | 0.0029 | 0.5 | 9.6 | 13α−15α | 13α−15α |
| | *C* | 3.20 | 1.49 | 0.0018 | 0.0020 | 1.3 | 5.2 | 13α−16α | 13α−16α |
| | *D* | 3.55 | 2.03 | 0.0209 | 0.0026 | 0.09 | 2.2 | 13α−17α | 13α−17α |
| | *E* | 4.00 | 2.38 | 0.0049 | 0.0196 | 0.3 | 0.2 | mixed α | 13α−18α |
| *syn*-**1**$^{+}$[h] | *A* | – | 0.38 | – | 0.0001 | – | >20 | – | 13α−14α |
| | *B* | – | 1.04 | – | 0.0003 | – | >20 | – | 13α−15α |
| | *C* | – | 1.48 | – | 0.0051 | – | 2.1 | – | 13α−16α |
| | *D* | – | 2.35 | – | 0.0025 | – | 1.7 | – | 13α−17α |
| | *E* | – | 2.54 | – | 0.0156 | – | 0.2 | – | 13α−18α |
| *anti*-**1**$^{+}$[h] | *A* | – | 0.53 | – | 0.0008 | – | >20 | – | 13α−14α |
| | *B* | – | 1.08 | – | 0.0015 | – | 13.3 | – | 13α−15α |
| | *C* | – | 1.53 | – | 0.0023 | – | 4.3 | – | 13α−16α |
| | *D* | – | 2.37 | – | 0.0028 | – | 1.5 | – | 13α−17α |
| | *E* | – | 2.49 | – | 0.0178 | – | 0.2 | – | 13α−18α |

[a] Vertical excitation energies in units of electronvolts. [b] Oscillator strengths. [c] Dominant configurations with expansion coefficients of >0.88. [d] From spin-unrestricted UCIS/6-311+G(2d,p) single-point calculations. [e] From time-dependent UB3LYP/6-311++G(3df,2p) single-point calculations. [f] UB3LYP/6-311+G(2d,p)-optimized geometry of the ground electronic state. [g] UCIS/6-311+G(2d,p)-optimized geometry of excited states *A*−*E*. [h] B3LYP/6-311+G(2d,p)-optimized geometry of the cation.

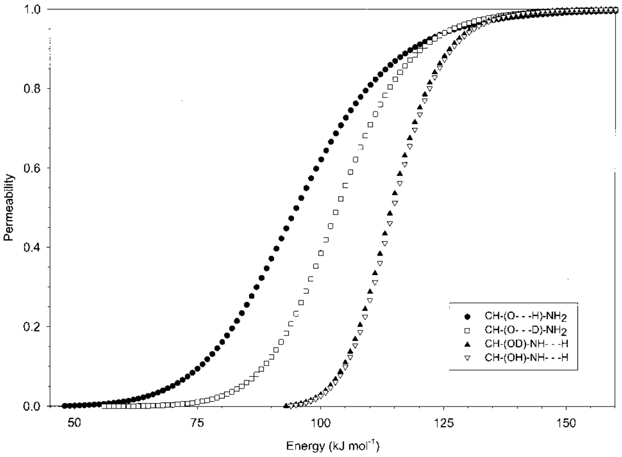

**Figure 10.** Potential energy barrier permeabilities in dissociations of **1** and **1a**.

barrier, was calculated as a function of internal energy, $E$ (eq 1).

$$G = \left\{\sinh^2\left[\pi\frac{\sqrt{2\mu E}}{\hbar}b\left(1+\sqrt{\frac{E-\Delta H_{\mathrm{rxn}}}{E}}\right)\right] - \sinh^2\left[\pi\frac{\sqrt{2\mu E}}{\hbar}b\left(1-\sqrt{\frac{E-\Delta H_{\mathrm{rxn}}}{E}}\right)\right]\right\} \Big/ \left\{\sinh^2\left[\pi\frac{\sqrt{2\mu E}}{\hbar}b\left(1+\sqrt{\frac{E-\Delta H_{\mathrm{rxn}}}{E}}\right)\right] + \cosh^2\left(\frac{1}{2}\pi\sqrt{\frac{32\mu b^2 V_0}{\hbar^2}-1}\right)\right\} \quad (1)$$

G2 energies were used for potential energy barriers ($V_0$) and reaction enthalpies ($\Delta H_{\mathrm{rxn}}$). The $b$ value was taken as $^1/_6$ of the bond length difference between the relaxed radical and transition state geometries, as determined by G2(MP2) mapping of the potential energy surface. As shown in Figure 10, tunneling will occur to a greater degree for both the O−H and O−D cleavages than for N−H cleavage in **1**, mainly due to the wider and higher energy barrier involved with N−H dissociation. In **1a**, tunneling is shifted to a higher energy for O−D dissociations, and to a slightly lower energy for N−H dissociation. The former result is due to an increased energy barrier and reaction enthalpy, and to a significant degree, the greater reduced mass $\mu$ for D. Reaction endothermicity for N−H cleavage actually is reduced in the presence of an O−D species (as in **1a**), leading to a slightly shifted permeability curve. Despite these shifts, at all reactant internal energies for which $E \leq V_0$, the barrier for the O−D bond dissociations is more permeable by tunneling than the barrier for the N−H bond dissociation. This implies that isotope effects on tunneling do not prefer N−H bond dissociation at transition state or lower energies.

**Addition of a Hydrogen Atom to Formamide.** While the branching ratios for competitive losses of hydrogen atoms from *syn*- and *anti*-**1** describe the intrinsic reactivity of these H atom adducts, H atom additions to **2** can lead to products other than **1**. The activation energies for H atom attacks at C, O, N, and H−C were therefore investigated computationally to assess the relative rates for the corresponding bimolecular reactions under thermal conditions at the high-pressure limit. H atom attacks at C and O in **2** result in additions producing **1** and **6**, respectively (eqs 2 and 3, respectively).

**TABLE 6: Relative Energies for Reactions of Hydrogen Atoms with Formamide**

| reaction | relative energy[a] G2(MP2) | G2 | CCSD(T)[b] | $E_{\mathrm{Arrh}}$[c] | log $A$[c] |
|---|---|---|---|---|---|
| $\mathbf{2} + \mathrm{H}^\bullet \rightarrow$ **TS1** | 62 | 59 | 51 | 51.8 | 13.04 |
| $\mathbf{2} + \mathrm{H}^\bullet \rightarrow$ *syn*-**1** | −31 | −35 | −47 | – | – |
| $\mathbf{2} + \mathrm{H}^\bullet \rightarrow$ **TS7** | 57 | 55 | 49 | 48.4 | 12.61 |
| $\mathbf{2} + \mathrm{H}^\bullet \rightarrow$ **6** | 14 | 13 | 2 | – | – |
| $\mathbf{2} + \mathrm{H}^\bullet \rightarrow$ **TS8** | 32 | 32 | 28.5 | 29.1 | 13.11 |
| $\mathbf{2} + \mathrm{H}^\bullet \rightarrow \mathrm{H_2NC{=}O^\bullet} + \mathrm{H_2}$ | −43 | −24 | −43 | – | – |
| $\mathbf{2} + \mathrm{H}^\bullet \rightarrow$ **TS9** | 90 | 89 | 80 | – | – |
| $\mathbf{2} + \mathrm{H}^\bullet \rightarrow \mathrm{HC{=}O^\bullet} + \mathrm{NH_3}$ | −32 | −31 | −37 | – | – |

[a] In units of kilojoules per mole. [b] With the aug-cc-pVTZ basis set. [c] From Arrhenius plots of rate constants based on CCSD(T) energies.

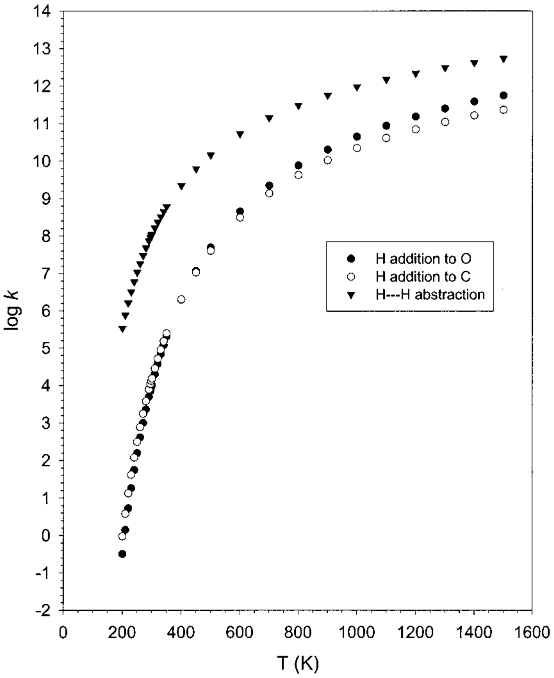

**Figure 11.** Thermal rate constants (log, cubic centimeters per mole per second$^{-1}$) for H atom reactions with **1**. Activation energies from CCSD(T)/aug-cc-pVTZ calculations.

$$\mathbf{2} + \mathrm{H}^\bullet \rightarrow \mathbf{TS1} \rightarrow syn\text{-}\mathbf{1} \quad (2)$$

$$\mathbf{2} + \mathrm{H}^\bullet \rightarrow \mathbf{TS7} \rightarrow \mathrm{H_2C(O^\bullet)NH_2}\ (\mathbf{6}) \quad (3)$$

$$\mathbf{2} + \mathrm{H}^\bullet \rightarrow \mathbf{TS8} \rightarrow \mathrm{O{=}C^\bullet NH_2} + \mathrm{H_2} \quad (4)$$

$$\mathbf{2} + \mathrm{H}^\bullet \rightarrow \mathbf{TS9} \rightarrow \mathrm{O{=}CH^\bullet} + \mathrm{NH_3} \quad (5)$$

H atom attack at the H−C bond in **2** results in elimination of $H_2$ and formation of an $\mathrm{O{=}CNH_2}$ radical (eq 4). H atom attack at the $NH_2$ group results in an elimination of ammonia to form the formyl radical, $\mathrm{HC{=}O^\bullet}$ (eq 5). The corresponding reaction and activation energies are summarized in Table 6. At all levels of theory used in this work, reaction 4 was the lowest-energy pathway; for example, $E_{\mathrm{TS}}$ = 28.5 kJ/mol from CCSD(T) calculations. Reactions 2 and 3 had similar activation barriers, 51 and 49 kJ/mol, respectively. Reaction 5 was the kinetically least favorable process that had a large activation barrier. Bimolecular rate constants (cubic centimeters per mole per second) from transition state theory calculations that are based on CCSD(T) energies are shown in Figure 11. Over a broad range of temperatures, reaction 4 was preferred by <1−2 orders of magnitude compared with reactions 2 and 3. Reaction 5 was negligibly slow and is therefore not shown in Figure 11. The relative rate constants calculated here agree qualitatively with previous pyrolysis[52] and pulse radiolysis studies[53] that showed preferential abstraction of the H−C hydrogen atom in formamide by a variety of radicals in the gas phase and solution.

Tunneling corrections to the rate constants were estimated from the Wigner formula[50,54] (eq 6)

$$\kappa = 1 + \frac{1}{24}\left(\frac{hc\nu}{kT}\right)^2 \qquad (6)$$

where $\nu$ is the imaginary frequency along the reaction coordinate in the transition state. Equation 6 provided transmission coefficients $\kappa$ of 2.1, 2.0, and 2.5 at 298 K for reactions 2−4, respectively. The reaction rate enhancements by H atom tunneling were therefore similar for reactions 2−4, and the overall kinetics were dominated by the corresponding activation energies which greatly preferred H atom abstraction.

## Conclusions

The combined experimental and computational study allows us to arrive at several conclusions. The amino(hydroxy)methyl radical (**1**) is the most stable isomer out of hydrogen atom adducts to formamide. A substantial fraction of radical **1** is stable when formed by collisional electron transfer in the gas phase. The main unimolecular dissociation of **1** is loss of the hydrogen atom from the hydroxyl group, which is also calculated to be the lowest-energy process. The kinetics of competitive losses of hydrogen atoms by cleavages of the O−H, N−H, and C−H bonds in **1**, as derived from variable-time measurements, showed a reasonably quantitative agreement with the relative rates calculated by RRKM theory. The energy driving the radical dissociations originates in part from large Franck−Condon effects on vertical electron capture. In addition, the observed dissociation kinetics and isotope effects can be interpreted by the formation upon electron capture of excited electronic states of **1** that undergo rate-determining, nonradiative transitions to the vibrationally excited ground state, followed by rapid dissociation.

The calculated kinetics of bimolecular reactions of formamide with hydrogen atoms indicate preferential abstraction of the hydrogen atom from the H−C group, while additions to the C═O group are substantially slower. This feature distinguishes formamide from other carboxamides, including peptides, that lack hydrogen atoms at the carbonyl carbon termini. Experimental and computational studies of radicals derived from more complex carboxamides that are more closely relevant to ECD are underway in this laboratory.

**Acknowledgment.** Support of this work by the National Science Foundation (Grants CHE-9712570 and CHE-0090930) is gratefully acknowledged. Support for the Computational Chemistry Facility was provided jointly by NSF-CRIF (Grant CH-9808182) and the University of Washington.

## References and Notes

(1) Steenken, S. *Chem. Rev.* **1989**, *89*, 503.

(2) Kochetkov, N. K.; Kudrjashov, L. I.; Chlenov, M. A. *Radiation Chemistry of Carbohydrates*; Pergamon Press: Oxford, 1979.

(3) Stubbe, J.; van der Donk, W. A. *Chem. Rev.* **1998**, *98*, 705.

(4) Khaselev, N.; Murphy, R. C. *Free Radical Biol. Med.* **2000**, *29*, 620. For a review, see: Crastes de Paulet, A., Douste-Blazy, L., Paoletti, R., Eds. *Free Radicals, Lipoproteins, and Membrane Lipids*; Plenum Press: New York, 1990.

(5) (a) Parast, C. V.; Wong, K. K.; Lewisch, S. A.; Kozarich, J. W.; Peisach, J.; Magliozzo, R. S. *Biochemistry* **1995**, *34*, 2393. (b) Babcock, G. T.; Espe, M.; Hoganson, C.; Lydakis-Simantiris, N.; McCracken, J.; Shi, W.; Styring, S.; Tommos, C.; Warncke, K. *Acta Chem. Scand.* **1997**, *51*, 533. (c) Bender, C. J.; Sahlin, M.; Babcock, G. T.; Barry, B. A.; Chandrashekar, T. K.; Salowe, S. P.; Stubbe, J.; Lindstroem, B.; Petersson, L.; Ehrenberg, A.; Sjoberg, B. M. *J. Am. Chem. Soc.* **1989**, *111*, 8076.

(6) (a) Sjoberg, B. M.; Reichard, P.; Graslund, A.; Ehrenberg, A. *J. Biol. Chem.* **1977**, *252*, 536. (b) Barry, B. A.; El-Deeb, M. K.; Sandusky, P. O.; Babcock, G. T. *J. Biol. Chem.* **1990**, *265*, 20139.

(7) (a) Tureček, F.; Carpenter, F. H.; Polce, M. J.; Wesdemiotis, C. *J. Am. Chem. Soc.* **1999**, *121*, 7955. (b) Tureček, F.; Carpenter, F. H. *J. Chem. Soc., Perkin. Trans 2* **1999**, 2315. (c) O'Hair, R. A. J.; Blanksby, S.; Styles, M.; Bowie, J. H. *Int. J. Mass Spectrom.* **1999**, *182/183*, 203. (d) Polce, M. J.; Wesdemiotis, C. *J. Am. Soc. Mass Spectrom.* **1999**, *10*, 1241.

(8) Zubarev, R. A.; Kelleher, N. L.; McLafferty, F. W. *J. Am. Chem. Soc.* **1998**, *120*, 3265.

(9) (a) Jeon, S.-J.; Raksit, A. B.; Gellene, G. I.; Porter, R. F. *J. Am. Chem. Soc.* **1985**, *107*, 4129. (b) Boldyrev, A. I.; Simons, J. *J. Chem. Phys.* **1992**, *97*, 6621.

(10) For reviews of NRMS techniques, see: (a) Wesdemiotis, C.; McLafferty, F. W. *Chem. Rev.* **1987**, *87*, 485. (b) Holmes, J. L. *Mass Spectrom. Rev.* **1989**, *8*, 513. (c) Turecek, F. *Org. Mass Spectrom.* **1992**, *27*, 1087. (d) Zagorevskii, D. V.; Holmes, J. L. *Mass Spectrom. Rev.* **1994**, *13*, 113. (e) Goldberg, N.; Schwarz, H. *Acc. Chem. Res.* **1994**, *27*, 347. (f) Turecek, F. *J. Mass Spectrom.* **1998**, *33*, 779. (g) Schalley, C. A.; Hornung, G.; Schroder, D.; Schwarz, H. *Chem. Soc. Rev.* **1998**, *27*, 91. (h) Zagorevski, D. V.; Holmes, J. L. *Mass Spectrom. Rev* **1999**, *18*, 87.

(11) (a) Shaffer, S. A.; Tureček, F. *J. Am. Chem. Soc.* **1994**, *116*, 8647. (b) Shaffer, S. A.; Tureček, F. *J. Am. Soc. Mass Spectrom.* **1995**, *6*, 1004. (c) Shaffer, S. A.; Sadilek, M.; Tureček, F. *J. Org. Chem.* **1996**, *61*, 5234. (d) Sadilek, M.; Tureček, F. *Chem. Phys. Lett.* **1996**, *263*, 203. (e) Nguyen, V. Q.; Sadílek, M.; Ferrier, J. G.; Frank, A. J.; Tureček, F. *J. Phys. Chem. A* **1997**, *101*, 3789. (f) Wolken, J. K.; Nguyen, V. Q.; Tureček, F. *J. Mass Spectrom.* **1997**, *32*, 1162. (g) Shaffer, S. A.; Tureček, F. *J. Am. Soc. Mass Spectrom.* **1997**, *8*, 1111. (h) Frøsig, L.; Tureček, F. *J. Am. Soc. Mass Spectrom.* **1998**, *9*, 242.

(12) Zubarev, R. A.; Kruger, N. A.; Fridriksson, E. K.; Lewis, M. A.; Horn, D. M.; Carpenter, B. K.; McLafferty, F. W. *J. Am. Chem. Soc.* **1999**, *121*, 2857.

(13) Shaffer, S. A.; Sadílek, M.; Tureček, F.; Hop, C. E. C. A. *Int. J. Mass Spectrom. Ion Processes* **1997**, *160*, 137.

(14) Tureček, F.; Polášek, M.; Frank, A. J.; Sadílek, M. *J. Am. Chem. Soc.* **2000**, *122*, 2361.

(15) (a) Burkey, T. J.; Castelhano, A. L.; Griller, D.; Lossing, F. P. *J. Am. Chem. Soc.* **1983**, *105*, 4701. (b) Hop, C. E. C. A.; Holmes, J. L. *Org. Mass Spectrom.* **1991**, *26*, 476. (c) Shaffer, S. A.; Tureček, F.; Cerny, R. L. *J. Am. Chem. Soc.* **1993**, *115*, 12117. (d) Lazarou, Y. G.; Papagiannakopoulos, P. *J. Phys. Chem.* **1993**, *97*, 9133. (e) Harvey, J. N.; Schroder, D.; Schwarz, H. *Bull. Soc. Chim. Belg.* **1997**, *106*, 447.

(16) (a) MacInnes, I.; Walton, J. C.; Nonhebel, D. C. *J. Chem. Soc., Perkin Trans. 2* **1987**, 1789. (b) Sana, M.; Leroy, G.; Peeters, D.; Younang, E. *THEOCHEM* **1987**, *36*, 325. (c) Leroy, G.; Sana, M.; Wilante, C. *THEOCHEM* **1991**, *74*, 37. (d) Armstrong, D. A.; Rauk, A.; Yu, D. *J. Am. Chem. Soc.* **1993**, *115*, 666.

(17) Nguyen, V. Q.; Tureček, F. *J. Mass Spectrom.* **1996**, *31*, 843.

(18) (a) Kuhns, D. W.; Tran, T. B.; Shaffer, S. A.; Tureček, F. *J. Phys. Chem.* **1994**, *98*, 4845. (b) Kuhns, D. W.; Tureček, F. *Org. Mass Spectrom.* **1994**, *29*, 463.

(19) Tureček, F.; Gu, M.; Shaffer, S. A. *J. Am. Soc. Mass Spectrom.* **1992**, *3*, 493.

(20) Protonation of formamide with strong gas-phase acids ($CH_5^+$, $N_2H^+$, etc.) yields mixtures of ions. For a detailed study, see: Lin, H.-Y.; Ridge, D. P.; Uggerud, E.; Vulpius, T. *J. Am. Chem. Soc.* **1994**, *116*, 2996.

(21) Frisch, M. J.; Trucks, G. W.; Schlegel, H. B.; Scuseria, G. E.; Robb, M. A.; Cheeseman, J. R.; Zakrzewski, V. G.; Montgomery, J. A.; Stratmann, R. E.; Burant, J. C.; Dapprich, S.; Millam, J. M.; Daniels, A. D.; Kudin, K. N.; Strain, M. C.; Farkas, O.; Tomasi, J.; Barone, V.; Cossi, M.; Cammi, R.; Mennucci, B.; Pomelli, C.; Adamo, C.; Clifford, S.; Ochterski, J.; Petersson, G. A.; Ayala, P. Y.; Cui, Q.; Morokuma, K.; Malick, D. K.; Rabuck, A. D.; Raghavachari, K.; Foresman, J. B.; Cioslowski, J.; Ortiz, J. V.; Stefanov, B. B.; Liu, G.; Liashenko, A.; Piskorz, P.; Komaromi, I.; Gomperts, R.; Martin, R. L.; Fox, D. J.; Keith, T.; Al-Laham, M. A.; Peng, C. Y.; Nanayakkara, A.; Gonzalez, C.; Challacombe, M.; Gill, P. M. W.; Johnson, B. G.; Chen, W.; Wong, M. W.; Andres, J. L.; Head-Gordon, M.; Replogle, E. S.; Pople, J. A. *Gaussian 98*, revision A.6; Gaussian, Inc.: Pittsburgh, PA, 1998.

(22) (a) Becke, A. D. *J. Chem. Phys.* **1993**, *98*, 1372, 5648. (b) Stephens, P. J.; Devlin, F. J.; Chabalowski, C. F.; Frisch, M. J. *J. Phys. Chem.* **1994**, *98*, 11623.

(23) Møller, C.; Plesset, M. S. *Phys. Rev.* **1934**, *46*, 618.

(24) Rauhut, G.; Pulay, P. *J. Phys. Chem.* **1995**, *99*, 14572.

(25) (a) Finley, J. W.; Stephens, P. J. *THEOCHEM* **1995**, *357*, 225. (b) Wong, M. W. *Chem. Phys. Lett.* **1996**, *256*, 391. (c) Scott, A. P.; Radom, L. *J. Phys. Chem.* **1996**, *100*, 16502.

(26) Curtiss, L. A.; Raghavachari, K.; Pople, J. A. *J. Chem. Phys.* **1993**, *98*, 1293.

(27) Pople, J. A.; Head-Gordon, M.; Raghavachari, K. *J. Chem. Phys.* **1987**, *87*, 5968.

(28) (a) Curtis, L. A.; Raghavachari, K.; Trucks, G. W.; Pople, J. A. *J. Chem. Phys.* **1991**, *94*, 7221. (b) Curtiss, L. A.; Raghavachari, K.; Pople, J. A. *J. Chem. Phys.* **1993**, *98*, 1293.

(29) Čížek, J. *Adv. Chem. Phys.* **1969**, *14*, 35.

(30) Purvis, G. D.; Bartlett, R. J. *J. Chem. Phys.* **1982**, *76*, 1910.

(31) Dunning, T. H., Jr. *J. Chem. Phys.* **1989**, *90*, 1007.

(32) (a) Schlegel, H. B. *J. Chem. Phys.* **1986**, *84*, 4530. (b) Mayer, I. *Adv. Quantum Chem.* **1980**, *12*, 189.

(33) Foresman, J. B.; Head-Gordon, M.; Pople, J. A.; Frisch, M. J. *J. Phys. Chem.* **1992**, *96*, 135.

(34) Stratmann, R. E.; Scuseria, G. E.; Frisch, M. J. *J. Chem. Phys.* **1998**, *109*, 8218.

(35) Zhu, L.; Hase, W. L. *Quantum Chemistry Program Exchange*; Indiana University: Bloomington, IN, 1994; Program QCPE 644.

(36) Frank, A. J.; Sadilek, M.; Ferrier, J. G.; Tureček, F. *J. Am. Chem. Soc.* **1997**, *119*, 12343.

(37) Zhu, L.; Hase, W. L. *Chem. Phys. Lett.* **1990**, *175*, 117.

(38) Levine, I. N. *Physical Chemistry*, 3rd ed.; McGraw-Hill: New York, 1988; p 839.

(39) Hunter, E. P.; Lias, S. G. *J. Phys. Chem. Ref. Data* **1998**, *27*, 413.

(40) Yu, D.; Armstrong, D. A.; Rauk, A. *Chem. Phys.* **1996**, *202*, 243.

(41) Ruttink, P. J. A.; Burgers, P. C.; Terlouw, J. K. *Int. J. Mass Spectrom. Ion Processes* **1995**, *145*, 35.

(42) McGibbon, G. A.; Burgers, P. C.; Terlouw, J. K. *Int. J. Mass Spectrom. Ion Processes* **1994**, *136*, 191.

(43) Johnson, R. D., III; Hudgens, J. W. *J. Phys. Chem.* **1996**, *100*, 19874.

(44) (a) Gonzalez, C.; Schlegel, H. B. *J. Chem. Phys.* **1989**, *90*, 2154. (b) Gonzalez, C.; Schlegel, H. B. *J. Phys. Chem.* **1990**, *94*, 5523.

(45) McMillen, D. F.; Golden, D. M. *Annu. Rev. Phys. Chem.* **1982**, *33*, 493.

(46) (a) Wolken, J. K.; Tureček, F. *J. Phys. Chem. A* **1999**, *103*, 6268. (b) Wolken, J. K.; Tureček, F. *J. Am. Chem. Soc.* **1999**, *121*, 6010.

(47) Uggerud, E. *Adv. Mass Spectrom.* **1995**, *13*, 53.

(48) From TD-B3LYP/6-311++G(3df,2p) single-point calculations on optimized ground state geometries.

(49) Robin, M. B.; Bovey, F. A.; Basch, H. In *The Chemistry of Amides*; Zabicky, J., Ed.; Wiley-Interscience: London, 1970; Chapter 1, pp 2−72, and references therein.

(50) Bell, R. P. *The Tunnel Effect in Chemistry*; Chapman and Hall: New York, 1980; pp 27−29.

(51) Eckart, C. *Phys. Rev.* **1930**, *35*, 1303.

(52) (a) Back, R. A.; Yokota, T. *Int. J. Chem. Kinet.* **1973**, *5*, 37, 1039. (b) Back, R. A.; Boden, J. C. *Trans. Faraday Soc.* **1971**, *67*, 88. (c) Boden, J. C.; Back, R. A. *Trans. Faraday Soc.* **1970**, *66*, 175. (d) Gray, P.; Leyshon, L. J. *Trans. Faraday Soc.* **1969**, *65*, 780.

(53) (a) Rustgi, S.; Riesz, P. *Int. J. Radiat. Biol. Relat. Stud. Phys., Chem. Med.* **1978**, *33*, 325. (b) Bielski, B. H. J.; Allen, A. O. *J. Am. Chem. Soc.* **1977**, *99*, 5931. (c) Behar, D. *J. Phys. Chem.* **1974**, *78*, 2660. (d) Symons, M. C. R.; Bower, H.; McRae, J. *J. Chem. Soc. A* **1971**, 2400. (e) Hayon, E.; Ibata, T.; Lichtin, N. N.; Simic, M. *J. Am. Chem. Soc.* **1971**, *93*, 5388. (f) Bosco, S. R.; Cirillo, A.; Timmons, R. B. *J. Am. Chem. Soc.* **1969**, *91*, 3140.

(54) Wigner, E. *Z. Phys. Chem. B* **1932**, *19*, 203.